Reprint

Millipede - MEMS-based Scanning-Probe Data-Storage System

E. Eleftheriou, T. Antonakopoulos, G. K. Binnig, G. Cherubini, M. Despont, A. Dholakia, U. Durig, M. A. Lantz, H. Pozidis, H. E. Rothuizen and P. Vettiger

IEEE Transactions on Magnetics

VOL. 39, NO. 2, MARCH 2003, pp. 938-945

Millipede—A MEMS-Based Scanning-Probe Data-Storage System

E. Eleftheriou, *Fellow, IEEE*, T. Antonakopoulos, *Senior Member, IEEE*, G. K. Binnig, G. Cherubini, *Senior Member, IEEE*, M. Despont, A. Dholakia, *Senior Member, IEEE*, U. Dürig, M. A. Lantz, H. Pozidis, *Member, IEEE*, H. E. Rothuizen, and P. Vettiger, *Fellow, IEEE*

***Abstract*—Ultrahigh storage densities of up to 1 Tb/in.^{2} or more can be achieved by using local-probe techniques to write, read back, and erase data in very thin polymer films. The thermomechanical scanning-probe-based data-storage concept called Millipede combines ultrahigh density, small form factor, and high data rate. After illustrating the principles of operation of the Millipede, a channel model for the analysis of the readback process is introduced, and analytical results are compared with experimental data. Furthermore, the arrangement of data-storage fields as well as dedicated fields for servo and timing control is discussed, and system aspects related to the readback process, multiplexing, synchronization, and position-error-signal generation for tracking are introduced. Finally, the application of (d, k) modulation coding as a means to further increase areal density is presented, and the effect on the user data rates discussed.**

***Index Terms*—Atomic force microscope, high-density data-storage system, MEMS, modulation coding, probe storage, servo control, thermomechanical write/read/erase, timing recovery.**

I. Introduction

TECHNIQUES that use nanometer-sharp tips for imaging and investigating the structure of materials down to the atomic scale, such as the atomic force microscope (AFM) and the scanning tunneling microscope (STM) [1]–[3], are suitable for the development of ultrahigh-density storage devices [4]–[11]. As the simple tip is a very reliable tool for the ultimate local confinement of interaction, tip-based storage technologies can be regarded as natural candidates for extending the physical limits that are being approached by conventional magnetic storage. The areal densities that today's magnetic recording technologies can achieve will eventually reach a limit imposed by the well-known superparamagnetic effect. Several proposals have been formulated to overcome this limit, for example the adoption of patterned magnetic media, for which, however, the biggest challenge remains the patterning of the magnetic disk in a cost-effective manner. On the other hand, data rates of 1 Gb/s or more are achieved by magnetic recording, whereas the mechanical resonant frequencies of the AFM cantilevers limit the data rates of a single cantilever to a few megabytes per second for AFM data storage. Moreover, the feedback speed and low tunneling currents limit STM-based storage approaches to even lower data rates. The solution for substantially increasing the data rates achieved by tip-based storage devices is to employ micro-electro-mechanical systems (MEMS)-based arrays of cantilevers operating in parallel, with each cantilever performing WRITE/READ/ERASE operations in an individual storage field.

A MEMS-actuated magnetic probe-based storage system is described in [12] and the references therein. In [12], a magnetic storage medium is positioned in the x/y plane, and writing is achieved magnetically by using an array of probe tips, each tip being actuated in the z-direction. In [13], an atomic resolution storage concept is described, in which electron field emitters are employed to change the state of a phase-change medium in a bit-wise fashion.

In this paper, the Millipede concept, described in detail in [7]–[11], to realize scanning-probe data storage is first reviewed. The Millipede exploits parallel operation of very large two-dimensional, e.g., 32×32, AFM cantilever arrays with integrated tips and WRITE/READ/ERASE functionality. Then, an equivalent model to characterize the readback signal from a thermomechanical sensor is introduced, and analytical results obtained using the model are compared with experimental data. The remainder of the paper is devoted to presenting various system aspects of a storage system based on the Millipede. In particular, position-error-signal (PES) generation for servo control as well as synchronization strategies are described, and modulation coding techniques suitable for probe-based data-storage devices are introduced.

II. Principles of Operation of the Millipede

The Millipede device shown in Fig. 1 is a highly parallel scanning-probe data-storage system. Information is stored as sequences of "indentations" and "no indentations" that are written on nanometer-thick polymer films using an array of AFM cantilevers. "Indentations" and "no indentations" will be also referred to as "logical marks." Each cantilever performs WRITE/READ/ERASE operations over an individual storage field with area on the order of 100×100 μm^2 [7]–[11]. Thermomechanical writing is achieved by applying a local force through the cantilever/tip to the polymer layer and simultaneously softening the polymer layer by local heating. Initially, the heat transfer from the tip to the polymer through the small contact area is very poor but improves as the contact area increases. This means that the tip must be heated to a relatively high temperature of about 400 °C to initiate the softening. Once softening has been initiated, the tip is pressed into the polymer,

Manuscript received July 3, 2002.

The authors are with IBM Research, Zurich Research Laboratory, 8803 Rüschlikon, Switzerland (e-mail: ele@zurich.ibm.com). T. Antonakopoulos was on sabbatical from the University of Patras, Department of Electrical and Computer Engineering, Patras 26500, Greece.

Digital Object Identifier 10.1109/TMAG.2003.808953

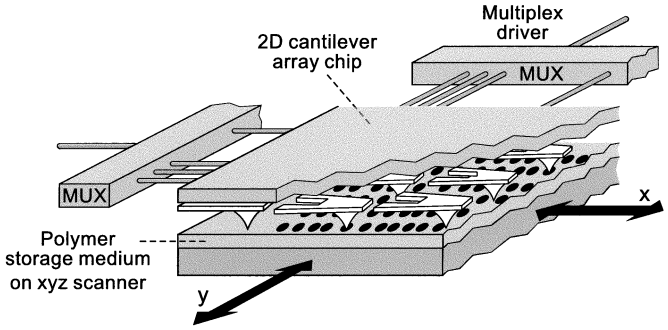

Fig. 1. Illustration of the Millipede concept.

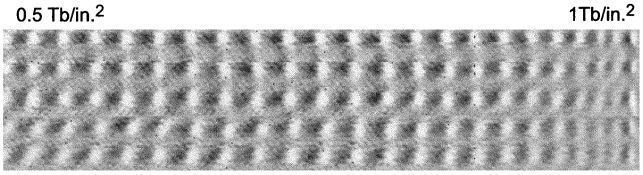

Fig. 2. Ultrahigh-density bit writing with areal densities approaching 1 Tb/in.^{2}.

and hence the indentation size is increased. Fig. 2 shows recent results from a single-lever experiment, where indentations are spaced as closely as 25 nm apart, resulting in areal densities up to 1 Tb/in.^{2}, although at a somewhat degraded WRITE/READ quality.

To read the written information, the heater cantilever originally used for writing is given the additional function of a thermal readback sensor by exploiting its temperature-dependent resistance. In general, the resistance increases nonlinearly with heating power/temperature from room temperature to a peak value at 500 °C–700 °C. The peak temperature is determined by the doping concentration of the heater platform, which ranges from 1×10^{17} to 2×10^{18} cm^{-3}. Above the peak temperature, the resistance drops as the number of intrinsic carriers increases because of thermal excitation. For sensing, the resistor is operated at about 350 °C, a temperature that is not high enough to soften the polymer as in the case of writing. The principle of thermal sensing is based on the fact that the thermal conductance between the heater platform and the storage substrate changes according to the distance between them. The medium between the heater platform and the storage substrate, in our case air, transports heat from the cantilever to the substrate. When the distance between cantilever and storage substrate is reduced as the tip moves into a bit indentation, the heat transport through the air becomes more efficient. As a result, the evolution of the heater temperature differs in response to a pulse applied to the cantilever. In particular, the maximum value achieved by the temperature is higher if there is no bit indentation. As the value of the variable resistance depends on the temperature of the cantilever, the maximum value achieved by the resistance will be lower as the tip moves into an indentation. Therefore, during the read process, the cantilever resistance reaches different values depending on whether the tip moves into an *indentation* (bit "1") or over a region *without an indentation* (bit "0"). The thermomechanical cantilever sensor, which transforms temperature into an electrical signal that carries information, is the electrical equivalent, to a first degree of approximation, of a variable resistance. A detection circuit must therefore sense a voltage that depends on the value of the cantilever resistance to decide whether a "1" or a "0" is written. The relative variation of thermal resistance is on the order of 10^{-5}/nm. Hence, a written bit "1" typically produces a relative change of the cantilever thermal resistance $\Delta R^{\Theta}/R^{\Theta}$ of about 10^{-4} to 5×10^{-4}. Note that the relative change of the cantilever electrical resistance is of the same order of magnitude. Thus, one of the most critical issues in detecting the presence or absence of an "indentation" is the high resolution required to extract the signal that contains the information about the bit being "1" or "0". The signal carrying the information can be regarded as a small signal superimposed on a very large offset signal. The large offset problem can be mitigated by resorting to a dedicated reference cantilever, as will be described in Section III.

Erasing of bits is achieved by exploiting to the so-called pile-up phenomenon, whereby rings of polymer appear around indentations as a result of the write process. If the ring of a new indentation is extended over the region of a previously written bit "1," then the depth of the previous indentation decreases markedly [9]. Therefore, by properly adjusting the distance between successive indentations, it is possible to achieve the function of erasing at the line or even bit level.

WRITE/READ operations depend on a mechanical parallel x/y scanning of either the entire cantilever array chip or the storage medium. The tip-medium contact is maintained and controlled globally, i.e., not on an individual cantilever basis, by using a feedback control for the entire chip, which greatly simplifies the system. Early results demonstrating the concept of the entire chip approach/leveling [14] indicate that overall chip tip-apex height control to within 500 nm is feasible. The stringent requirement for tip-apex uniformity over the entire chip is determined by the uniform force required to reduce tip and medium wear due to large force variations resulting from large tip-height nonuniformities [15]. As the Millipede tracks the entire array without individual lateral cantilever positioning, thermal expansion of the array chip has to be small or well controlled. For a 3×3 mm^2 silicon array area and tip-position accuracy of 10 nm, the chip temperature has to be controlled to within about 1 °C. This is ensured by four temperature sensors in the corners of the array and heater elements on each side of the array. Thermal expansion considerations are a strong argument for a two-dimensional (2-D) instead of a one-dimensional (1-D) array arrangement, which would make a chip 32 times longer for a 32×32 array of cantilevers.

Efficient parallel operations of large 2-D arrays can be achieved by a row/column time-multiplexed addressing scheme similar to that implemented in DRAMs. In the case of Millipede, the multiplexing scheme is used to address the array column by column with full parallel WRITE/READ operation within one column [9]. In particular, readback signal samples are obtained by applying an electrical read pulse to the cantilevers in a column of the array, low-pass filtering the cantilever response signals, and finally sampling the filter output signals. This process is repeated sequentially until all

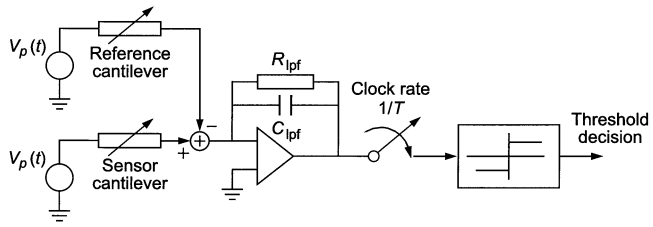

Fig. 3. Block diagram of the detection circuit.

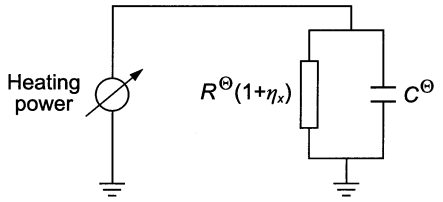

Fig. 4. RC-equivalent thermal model of the heat transfer process.

columns of the array have been addressed and then restarted from the first column. The time between two pulses applied to the cantilevers of the same column corresponds to the time it takes for a cantilever to move from one bit position to the next. An alternative approach is to access all or a subset of the cantilevers simultaneously without resorting to the row/column multiplexing scheme. Clearly, the latter scheme yields higher data rates, whereas the former leads to lower implementation complexity of the channel electronics.

III. Read Channel Model

In this section, we consider the readback channel for a single cantilever, scanning a storage field where bits are written as indentations or no indentations in the storage medium. As discussed above, a cantilever is modeled as a variable resistance that depends on the temperature at the cantilever tip. The model of the read channel, which serves for the design and the analysis of the detection system, is illustrated in Fig. 3.

To evaluate the evolution of the temperature of a heated cantilever during the read process, we resort to a simple RC-equivalent thermal circuit, illustrated in Fig. 4, where $(1+\eta_x)R^{\Theta}$ and C^{Θ} denote the thermal resistance and capacitance, respectively. The parameter $\eta_x = \Delta R^{\Theta}(x)/R^{\Theta}$ indicates the relative variation of thermal resistance that results from the small change in air-gap width between the cantilever and the storage medium. The subscript x indicates the distance in the direction of scanning from the initial point. Therefore, the parameter η_x will assume the largest absolute value when the tip of the cantilever is located at the center of an indentation. The heating power that is dissipated in the cantilever heater region is expressed as

$$P^e(t,\Theta(t,x)) = \frac{V_C^2(t)}{R^e(\Theta(t,x))} \tag{1}$$

where $V_C(t)$ is the voltage across the cantilever, $\Theta(t,x)$ is the cantilever temperature, and $R^e(\Theta(t,x))$ is the temperature-dependent cantilever resistance.

As the heat-transfer process depends on the value of thermal resistance and on the read pulse waveform, the cantilever temperature $\Theta(t,x)$ depends on time t and distance x. However, because the time it takes for the cantilever to move from the center of a logical mark to the next is greater than the duration of a read pulse, we assume that $\Theta(t,x)$ does not vary significantly as a function of x while a read pulse is being applied, and that it decays to the ambient temperature Θ_0 before the next pulse is applied. Therefore, the evolution of the cantilever temperature in response to a pulse applied at time $t_0 = x_0/v$, at a certain distance x_0 from the initial point of scanning and for a certain constant velocity v of the scanner, obeys a differential equation that is expressed as

$$\Theta'(t,x_0) + \frac{1}{(1+\eta_{x_0})R^{\Theta}C^{\Theta}}(\Theta(t,x_0)-\Theta_0) = \frac{1}{C^{\Theta}}\frac{V_C^2(t)}{R^e(\Theta(t,x_0))} \tag{2}$$

where $\Theta'(t,x_0)$ denotes the derivative of $\Theta(t,x_0)$ with respect to time.

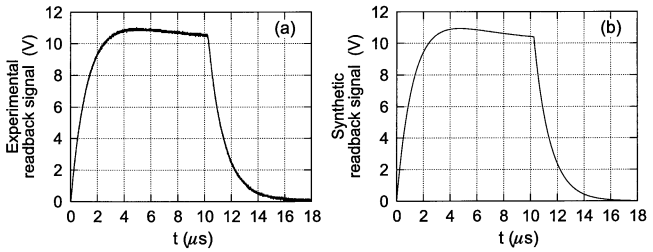

(a) (b)

Fig. 5. (a) Experimental and (b) synthetic readback signal for $\tau = 10.25\ \mu$s.

With reference to the block diagram of the read channel illustrated in Fig. 3, the source generates the read pulse $V_P(t)$ that is applied to the cantilever. Clearly, because of the virtual ground at the operational amplifier input, the voltage $V_C(t)$ across the cantilever variable resistance is equal to $V_P(t)$. Furthermore, the active low-pass RC detector filter, where $R_{\rm lpf}$ and $C_{\rm lpf}$ denote the resistance and capacitance of the low-pass filter, respectively, is realized using an ideal operational amplifier that exhibits infinite input impedance, zero output impedance, and infinite frequency-independent gain. Therefore, the readback signal $V_o(t,x_0)$ obtained at the low-pass filter output in response to the applied voltage $V_P(t) = A\,\mathrm{rect}((t-T_0)/\tau)$, where

$$\mathrm{rect}\left(\frac{t}{\tau}\right) = \begin{cases} 1, & \text{if } 0 \le t \le \tau \\ 0, & \text{otherwise} \end{cases} \tag{3}$$

and A denotes the pulse amplitude, obeys the differential equation

$$V_o'(t,x_0) = \frac{1}{R_{\rm lpf}C_{\rm lpf}}\left(-V_o(t,x_0) + \frac{R_{\rm lpf}}{R^e(\Theta(t,x_0))}V_P(t)\right). \tag{4}$$

As the voltage at the output of the low-pass filter depends on the value of the variable resistance $R^e(\Theta(t,x_0))$, the readback signal is determined by solving jointly (2) and (4), with initial conditions $\Theta(t_0,x_0) = \Theta_0$ and $V_o(t_0,x_0) = 0$. For example, a comparison between experimental and synthetic readback signals is shown in Figs. 5 and 6 for a time constant of the low-pass filter $\tau_{\rm lpf} = 1.18\ \mu$s, and two values of the duration of the applied rectangular pulse. For a given cantilever design the function $R^e(\Theta)$ is determined experimentally. Finally, the param-

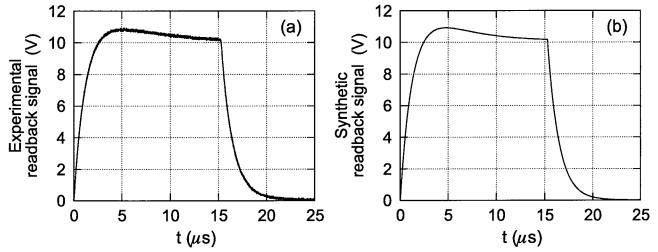

(a) (b)

Fig. 6. (a) Experimental and (b) synthetic readback signal for $\tau = 15.25\ \mu$s.

eters R^{Θ} and C^{Θ} used in the simple readback channel model are obtained via simulated annealing, where the cost function is given by the mean-square error between experimental and synthetic signals at the low-pass-filter output.

Assuming that ideal control of the scanner is performed such that the time of application of a read pulse corresponds either to the cantilever being located at the center of an indentation for detecting a bit "1," or away from an indentation for detecting a bit "0," two possible responses are obtained at the output of the low-pass filter as solutions of (2) and (4), which we denote by $V_{o,1}(t, x_0)$ and $V_{o,0}(t, x_0)$, respectively. By sampling the readback signal at the instant $t_s = t_0 + \tau$, simple threshold detection may in principle be applied to detect a written bit, where the value of the threshold is given by

$$V_{\mathrm{Th}} = \frac{1}{2}\left[V_{o,1}(t_s, x_0) + V_{o,0}(t_s, x_0)\right]. \tag{5}$$

As mentioned in Section II, one of the most critical issues in detecting the presence or absence of an indentation is the high resolution required to extract the small signal $V_{o,1}(t_s, x_0) - V_{o,0}(t_s, x_0)$ that contains the information about the bit being "1" or "0," superimposed on the offset signal $V_{o,0}(t, x_0)$. As illustrated in Fig. 3, this problem can be solved by generating a reference signal $V_{o,\mathrm{ref}}(t, x_0)$ by applying the read pulse $V_P(t)$ at time $t = t_0$ to a cantilever scanning a storage field where no indentation is written, and subtracting it from the readback signal. The readback signal is thus given by

$$\tilde{V}_o(t, x_0) = V_o(t, x_0) - V_{o,\mathrm{ref}}(t, x_0) \tag{6}$$

and the threshold is set at $\tilde{V}_{\mathrm{Th}} = (1/2)[V_{o,1}(t_s, x_0) - V_{o,0}(t_s, x_0)]$. A VLSI implementation of the detection scheme analyzed here is presented in [16].

Consider now read pulses of duration τ that are periodically applied at instants $t_n = nT$, where $1/T$ denotes the symbol rate. Assuming that at every time instant a new pulse is applied the response of the previous pulse has vanished, and that the temperature of the cantilever has approached the ambient temperature, i.e., $V_o(t_n, x_n) = 0$ and $\Theta(t_n, x_n) = \Theta_0$, then the analysis presented above still holds. In particular, the readback signal samples obtained in response to N pulses applied to the cantilever for detecting a sequence of N binary written symbols are expressed as

$$s(t_{s,n}) = \tilde{V}_o(t_{s,n}, x_n), \quad t_{s,n} = nT + \tau, \quad n = 0, \ldots, N-1 \tag{7}$$

where $\tilde{V}_o(t, x_n)$ is given by (6) for pulses applied at time t_n and at distance $x_n = nTv$, $n = 0, \ldots, N-1$, from the initial point of scanning. Note that the functions $V_o(t, x_n)$ and $V_{o,\mathrm{ref}}(t, x_n)$ in (6) are given by the solution of (2) and (4) for $\eta_x = \Delta R^{\Theta}(x_n)/R^{\Theta}$ and $\eta_x = 0$, respectively.

The readback signal (6) at the output of the low-pass filter is observed in the presence of additive noise. Therefore, the readback signal for the detection of the nth binary symbol is given by

$$r(t_{s,n}) = s(t_{s,n}) + w(t_{s,n}) \tag{8}$$

where $w(t)$ denotes the noise signal. The components of the noise signal that must be taken into account are thermal noise (Johnson's noise) from the sensor and the reference cantilever resistances, which reach a temperature of about $\Theta_1 = 350°\mathrm{C}$ during the read process, and from the low-pass filter resistance, as well as noise from equivalent noise sources in the operational amplifier. The signal-to-noise ratio (SNR) at the detection point due to these noise components is expressed as

$$\mathrm{SNR} = 10\log_{10}\left(\frac{\tilde{V}_{\mathrm{Th}}^2}{\sigma_w^2}\right) \tag{9}$$

where the variance of the noise is approximated, as shown in (10) at the bottom of the page, with $k = 1.38 \times 10^{-23}$ J/K is the Boltzmann constant and $W_{\mathrm{OA}}(f)$ denotes the equivalent input-voltage noise-power spectral density of the operational amplifier. For typical values of the system parameters, an SNR in the range of 16 to 20 dB is obtained. However, note that besides thermal noise, also medium-related noise affects the overall system performance.

The above analysis together with the assumption that the indentations have a regular shape lead to a simple synthetic model for the simulation of the readback signal. In [9], a visco-elastic model of bit writing is described that yields a regular indentation shape. Alternatively, simple functions of the raised-cosine type can be used to approximately describe the shape of indentations. Fig. 7 illustrates the experimental and synthetic readback signals obtained along a data track. The waveforms shown in Fig. 7 have been obtained by applying pulses at the oversampling rate of q/T, where q denotes the oversampling factor.

IV. System Aspects

In this section, we describe various aspects of a storage system that employs the Millipede concept. Each cantilever can write data to and read data from a dedicated area of the

$$\sigma_w^2 = \int_{-\infty}^{+\infty} \frac{\left[4k\Theta_1 R^e(\Theta_1) + W_{\mathrm{OA}}(f)\right]\left(\frac{R_{\mathrm{lpf}}}{R^e(\Theta_1)}\right)^2 + 2k\Theta_0 R_{\mathrm{lpf}}}{\left|1 + j2\pi f \tau_{\mathrm{lpf}}\right|^2} df \tag{10}$$

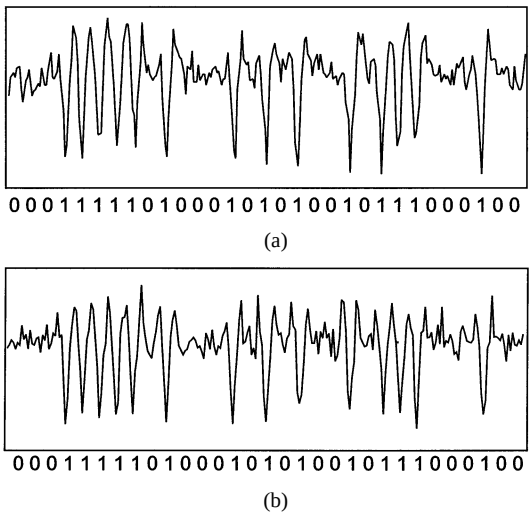

Fig. 7. Comparison between (a) the readback signal obtained experimentally along a data track and (b) the readback signal obtained by the synthetic model.

polymer substrate, called a *storage field*. As mentioned above, in each storage field the presence (absence) of an indentation corresponds to a logical "1" ("0"). All indentations are nominally of equal depth and size. The logical marks are placed at a fixed horizontal distance from each other along a data track. We refer to this distance, measured from logical mark center to logical mark center, as the *bit pitch* (BP). The vertical (cross-track) distance between logical mark centers, the *track pitch* (TP), is also fixed. To read and write data the polymer medium is moved under the (stationary) cantilever array at a constant velocity.

A robust way to achieve synchronization and servo control in an x/y-actuated large 2-D array is by reserving a small number of storage fields exclusively for timing recovery and servo-control purposes. Because of the large number of levers in the Millipede, this solution is advantageous in terms of overhead compared with the alternative of timing and servo information being embedded in all data fields.

A. PES Generation for the Servo Loop

With logical marks as densely spaced as in the Millipede, accurate track following becomes a critical issue. Track following means controlling the position of each tip such that the tip is always positioned over the center of a desired track during reading. During writing, the tip position should be such that the written marks are aligned in a predefined way. In electromechanical systems, track following is performed in a servo loop, which is driven by an appropriate error signal, called PES. Ideally, its magnitude is a direct estimate of the vertical (cross-track) distance of the tip from the track centerline, and its polarity indicates the direction of this offset.

Several approaches exist to generate a PES for AFM-based storage devices [6]. However, based on the results reported, none of these methods can achieve the track-following accuracy required for the Millipede system. The quality of the PES directly affects the stability and robustness of the associated tracking servo loop [17].

Here, we describe a method for generating a uniquely decodable PES for the Millipede system. The method is based

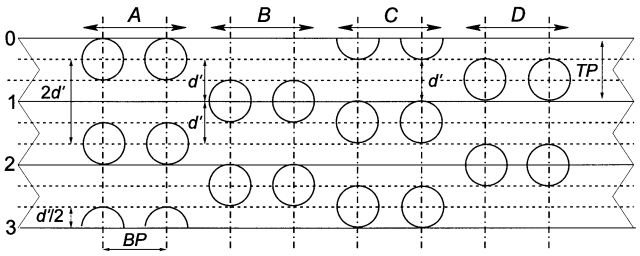

Fig. 8. Servo burst configuration.

on the concept of mutually vertically displaced *bursts*, arranged in such a way as to produce two signals in quadrature, which can be combined to provide a robust PES. This concept is borrowed from magnetic recording [17]; however, servo marks, as opposed to magnetic transitions, are placed in bursts labeled A and B for the in-phase signal and C and D for the quadrature signal. The centers of servo marks in burst B are vertically offset from mark centers in burst A by d' units of length. This amount of vertical spacing is related to the diameter of the written marks. The same principle applies to marks in the quadrature bursts C and D, with the additional condition that mark centers in burst C are offset by $d'/2$ units from mark centers in A in the cross-track direction. The latter condition is required in order to generate a quadrature signal. The configuration of servo bursts is illustrated in Fig. 8 for a case where $\mathrm{TP} = 3d'/2$. Although each burst typically consists of many marks to enable averaging of the corresponding readout signals, only two marks per burst are shown here to simplify the presentation. The solid horizontal lines depict track centerlines, and circles represent written marks, which are modeled as perfect conical indentations on the polymer storage surface.

To illustrate the principle of PES generation let us assume that marks in all bursts are spaced BP units apart in the longitudinal direction, and that sampling occurs exactly at mark centers, so that timing is perfect.[1] Referring to Fig. 8, let us further assume that the cantilever/tip is located on the line labeled "0" and moves vertically toward line "3," in a line crossing the centers of the left-most marks in burst A (shown as a dashed-dotted line). The tip moves from the edge of the top mark toward its center, then toward its bottom edge, then to a blank space, again to a mark, and so on. The readout signal magnitude decreases linearly with the distance from the mark center and reaches a constant, background level value at a distance greater than the mark radius from the mark center according to the adopted (conical mark) model. To synthesize the in-phase signal, the readout signal is also captured as the tip (conceptually) moves in a vertical line crossing the mark centers of burst B (dashed-dotted line in Fig. 8). The in-phase signal is then formed as the difference $\bar{A} - \bar{B}$, where $\bar{A}$ and $\bar{B}$ stand for the measured signal amplitudes in bursts A and B, respectively. This signal is represented by the line labeled "I" in Fig. 9. It has zero crossings at integer multiples of d', which do not generally correspond to track centers because we set $\mathrm{TP} = 3d'/2$ in this example. Therefore, the I-signal is not a valid PES in itself. This is why

[1]We note here that the assumption of perfect timing is made only for the purpose of illustration. In actual operation, sampling is performed with the aid of a timing recovery loop, as described in Section IV-B.

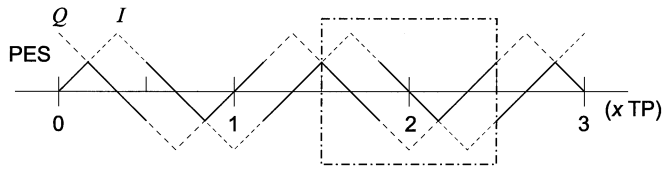

Fig. 9. Ideal position-error signal.

in this case the quadrature (Q) signal becomes necessary. The Q-signal is generated from the servo readback signals of bursts C and D as $\bar{C} - \bar{D}$ and is also shown in Fig. 9 (Q-curve). Note that it exhibits zero crossings at points where the I-signal has local extrema.

A certain combination of the two signals (I and Q), shown as solid lines in Fig. 9, has zero crossings at all track center locations and constant (absolute) slope, which qualifies it as a valid PES. However, this PES exhibits zero crossings at all integer multiples of $d'/2$. For our example of $\mathrm{TP} = 3d'/2$, three such zero crossings exist in an area of width equal to TP around any track centerline. This fact, however, does not hamper unique position decoding. At even-numbered tracks, it is the zero of the *in-phase* signal that indicates the track center. The zeros of the quadrature signal, in turn, can be uniquely mapped into a position estimate by examining the polarity of the in-phase signal at the corresponding positions. This holds for any value of the combined PES within an area of width equal to TP around each current track centerline. The signals exchange roles for odd-numbered tracks. The current track number, which is known *a priori* from the seek operation, is used to determine the mode of operation for the position demodulation procedure.

The principle of PES generation based on servo marks has been verified experimentally. For this purpose, A, B, C, and D bursts were written by an AFM cantilever/tip on an appropriate polymer medium consisting of a polymer coating on top of a silicon substrate. The bit pitch was set to 42 nm, and the track pitch was taken to be approximately equal to d', the cross-track distance between $A\,(C)$ and $B\,(D)$ bursts. An image created by reading the written pattern with the same cantilever is shown in Fig. 10. Shaded areas indicate indentations. The readout signal from the cantilever was also used for servo demodulation, as described above. The resulting in-phase and quadrature signals are shown in Fig. 11. The track centerlines are indicated by vertical dotted lines in the graph.

It can be observed that the zero-crossings of the in-phase signal are closely aligned with the track centerlines and also with the minima and maxima of the quadrature signal, as required for unique position decoding across all possible cross-track positions, at least in cases where $TP \neq d'$. Moreover, the PES slope is nearly linear along a cross-track width of one track pitch around each track center, as $TP \approx d'$ in this case, although deviations from the ideal signal shape exist. These deviations occur mainly because written indentations do not have perfect conical shapes and also because of media noise due to the roughness of the recording medium. Nevertheless, the experimentally generated error signals indicate that the proposed concept is valid and promising. Specifically, the results indicate that servo self-writing is feasible, that servo demodulation is almost identical to data readout and can be performed by any cantilever without special provisions, and that the PES generated closely approximates the desirable features described earlier.

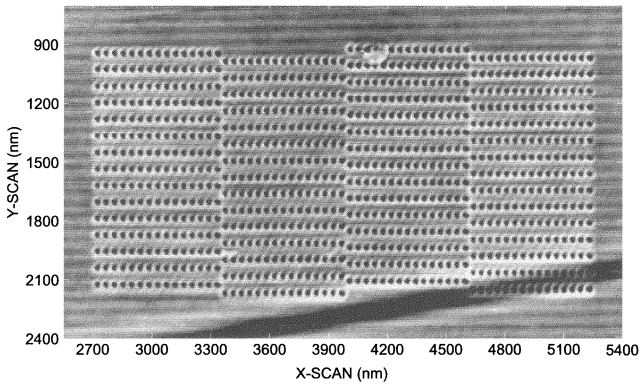

Fig. 10. Experimental A, B, C, and D servo bursts ($\mathrm{BP} = 42$ nm).

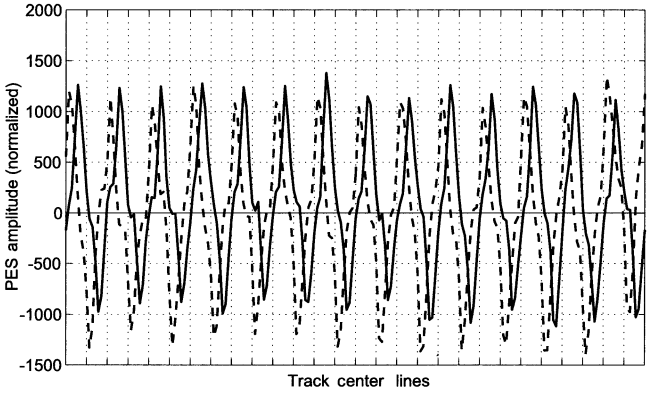

Fig. 11. Demodulated in-phase (solid line) and quadrature (dashed line) PES based on the servo burst of Fig. 10.

B. Timing Recovery

Similarly to obtaining servo information based on using dedicated servo fields, we employ separate dedicated clock fields for recovery of timing information. The concept is to have continuous access to a pilot signal for synchronization, after initial phase acquisition and gain estimation. The recovered clock is then distributed to all remaining storage fields to allow reliable detection of random data. Initial phase acquisition is obtained by a robust correlation algorithm, gain estimation is based on averaging of the readback signal obtained from a predefined stored pattern, and finally tracking of the optimum sampling phase is achieved by a second-order digital loop.

At the beginning of the read process, several signal parameters need to be estimated prior to data detection. Besides the clock phase and frequency, it is necessary to estimate the gain of the overall read channel. To solve the problem of initial estimation of signal parameters prior to data detection, the sequence written in the clock field consists of a preamble, followed by a pattern of all "1"s for tracking the optimum sampling phase during the detection of random data. The transition between the preamble and the pattern of all "1"s must be reliably detected, as it indicates the start of data records to the remaining storage fields. Assuming that the initial frequency offset is within a predetermined small range, usually 1000 part-per-million (PPM),

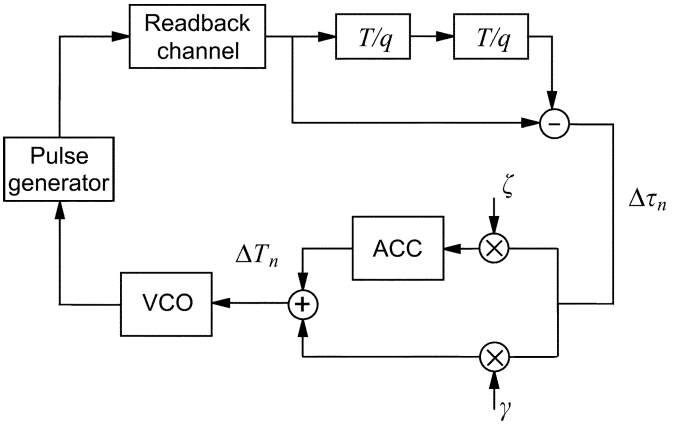

Fig. 12. Second-order loop for tracking the optimum sampling phase.

we distinguish the tasks that are needed for timing recovery as follows:

- acquisition of the optimum sampling phase;
- estimation of the overall channel gain needed for threshold detection;
- detection of the transition between the preamble and the pattern of all "1"s;
- tracking of the optimum sampling phase.

At the beginning of the acquisition process, an estimate of the optimum sampling phase is obtained by resorting to a correlation method. We rely on the knowledge of the preamble and of an ideal reference-channel impulse response, which closely resembles the actual impulse response (see Section III). The channel output samples obtained at the oversampling rate q/T are first processed by removing the dc-offset, then averaging, and finally correlating the resulting sequence with the reference impulse response to determine the phase estimate.

After determining the estimate of the optimum sampling phase, an estimate of the overall channel gain is obtained by averaging the amplitude of the channel output samples at the optimum sampling instants. The gain estimate is obtained from an initial segment of the preamble corresponding to an "all one" binary pattern. As mentioned earlier, it is necessary that the end of the preamble is indicated by a "sync" pattern, which marks the transition between acquisition mode and tracking mode. Detection of the "sync" pattern is also based on a robust correlation method. After the "sync" pattern, an "all one" pattern, as in the case of robust phase acquisition and gain estimation, is employed for tracking. The "all one" pattern corresponds to regularly spaced indentations, which convey reliable timing information.

Tracking of the optimum sampling phase is achieved by the second-order loop configuration shown in Fig. 12. Assuming data detection is performed at instants that correspond to integer multiples of the oversampling factor q, the deviation of the sampling phase from the optimum sampling phase is estimated as

$$\Delta\tau_n = r(t_{s,nq+1/q}) - r(t_{s,nq-1/q}). \tag{11}$$

This estimate of the phase deviation is input to a second-order loop filter, which provides an output given by

$$\Delta T_n = u_n + \gamma\Delta\tau_n \tag{12}$$

TABLE I
AREAL DENSITY AND STORAGE CAPACITY

Coding	linear density (kpbi)	track density (ktpi)	areal density (Gb/in.^{2})	capacity (GB)
uncoded	847	847	717	1.21
$(d=1, k\geq 6)$	1129	847	956	1.61
$(d=2, k>6)$	1269	847	1075	1.81

where the discrete-time integrator is recursively updated as

$$u_{n+1} = u_n + \zeta\Delta\tau_n. \tag{13}$$

The loop-filter output then determines the control signal for a voltage-controlled oscillator (VCO).

Note that a similar concept for timing recovery can also be applied if no separate clock field is available. In this case, the timing information is extracted from the random user data on each storage field.

C. Considerations on Capacity and Data Rate

The ultimate locality provided by nanometer-sharp tips represents the pathway to the high areal density that will be needed in the foreseeable future. The intrinsic nonlinear interactions between closely spaced indentations, however, determine the minimum distance between successive indentations and hence the areal density.

Today's storage capacity of a Millipede-based storage device can be further increased by applying modulation or constrained codes that impose restrictions on the number of consecutive "1"s and "0"s in the encoded data sequence. This class of codes is generally known as run-length-limited (RLL) (d, k) codes [18]. The code parameters d and k are nonnegative integers with $k > d$, where d indicates the minimum number of "0"s between two "1"s and k indicates the maximum number of zeros between two "1"s. For the Millipede application, where dedicated clock fields are used, the k parameter can be set to infinity, thereby facilitating the code-design process. The quantity $(d+1)R$, where R denotes the rate of the (d, k) code, is a direct measure of the increase in linear recording density. Clearly, the packing density can be made arbitrarily large by increasing d. On the other hand, large values of d lead to codes with very low rate, which implies high recording symbol rates, thus rendering these codes impractical for storage systems that are limited by the clock speed. The choice of $d = 1$ and $k \geq 6$ guarantees the existence of a code with rate $R = 2/3$. Use of $(d = 1, k \geq 6)$ modulation coding reduces the bit distance by half while maintaining constant the pitch between "1"s, thereby increasing the linear density by a factor of 4/3. Similarly, the choice of $d = 2$ and $k > 6$ guarantees the existence of a code with rate $R = 1/2$. Use of $(d = 2, k > 6)$ modulation coding reduces the bit distance to a third while maintaining constant the pitch between "1"s, thereby increasing the linear density by a factor of 3/2. Table I shows the achievable areal densities and storage capacities for a (32×32) cantilever array with 1024 storage fields, each having an area of $100 \times 100\ \mu\text{m}^2$, resulting in total storage area of $3.2 \times 3.2\ \text{mm}^2$. The indentation pitch and the track pitch are set equal to 30 nm. Finally, for the computation of the storage

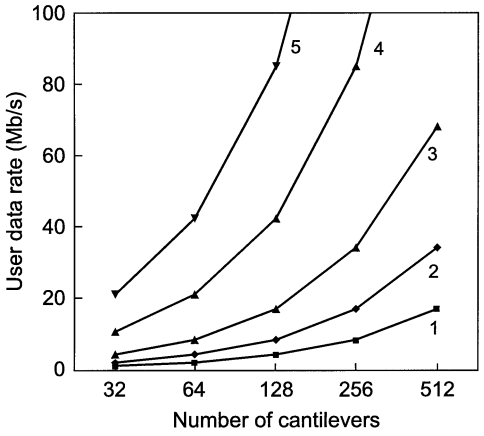

Fig. 13. User data rate versus number of active cantilevers for the ($d = 1$, $k \geq 6$) coding scheme. Curve 1: $T = 20$ μs; curve 2: $T = 10$ μs; curve 3: $T = 5$ μs; curve 4: $T = 2$ μs, and curve 5: $T = 1$ μs.

capacity an overall efficiency of 85% has been assumed, taking into account the redundancy of the outer error-correction coding as well as the presence of dedicated servo and clock fields.

Fig. 13 shows the user data rate as a function of the total number of cantilevers accessed simultaneously, for various symbol rates and a ($d = 1$, $k \geq 6$) modulation coding scheme. For example, for a (32×32) cantilever array, a system designed to access a maximum of 256 cantilevers every $T = 5$ μs provides a user data rate of 34.1 Mb/s. Alternatively, by resorting to the row/column multiplexing scheme with $T = 80$ μs a data rate of 8.5 Mb/s is achieved.

V. Conclusion

The Millipede has the potential to achieve ultrahigh storage areal densities on the order of 1 Tb/in.^{2}. The high areal storage density, small form factor, and low power consumption render Millipede a very attractive candidate for future storage technology for mobile applications, as it offers several gigabytes of capacity at data rates of several megabytes per second. Dedicated servo and timing fields allow reliable system operation with a very small overhead. The read channel model introduced in this paper provides the methodology for analyzing system performance and assessing various aspects of the detection and servo/timing algorithms that are key to achieving the system reliability required by the applications envisaged.

Acknowledgment

The authors would like to thank their colleagues P. Bächtold, U. Drechsler, B. Gotsmann, W. Häberle, T. Loeliger, and R. Stutz for technical contributions and P. F. Seidler and W. Bux for their support. They would also like to thank S. Sri-Jayantha, A. Sharma, and H. Dang of the IBM T. J. Watson Research Center, T. Albrecht of the IBM Almaden Research Center, currently at the IBM Zurich Research Laboratory, and B. Pogge and R. Yu of the IBM Microelectronics Division, for their contributions to this work.

References

[1] G. Binnig, H. Rohrer, C. Gerber, and E. Weibel, "7 × 7 reconstruction on Si(111) resolved in real space," *Phys. Rev. Lett.*, vol. 50, no. 2, pp. 120–123, 1983.

[2] G. Binnig, C. F. Quate, and C. Gerber, "Atomic force microscope," *Phys. Rev. Lett.*, vol. 56, no. 9, pp. 930–933, 1986.

[3] H. J. Mamin, L. S. Fan, S. Hoen, and D. Rugar, "Tip-based data storage using micromechanical cantilevers," *Sensors Actuators A*, vol. 48, pp. 215–219, 1995.

[4] C. F. Quate, "Method and means of data storage using tunnel current data readout," US Patent 4 575 822, 1986.

[5] H. J. Mamin *et al.*, "High-density data storage using proximal probe techniques," *IBM J. Res. Develop.*, vol. 39, pp. 681–700, 1995.

[6] H. J. Mamin, R. P. Ried, B. D. Terris, and D. Rugar, "High-density data storage based on the atomic force microscope," *Proc. IEEE*, vol. 87, pp. 1014–1027, 1999.

[7] M. Despont *et al.*, "VLSI-NEMS chip for AFM data storage," in *Tech. Dig. 12th IEEE Int. Micro Electro Mechanical Systems Conf. "MEMS '99"*, 1999, pp. 564–569.

[8] P. Vettiger *et al.*, "The 'Millipede'—More than one thousand tips for future AFM data-storage," *IBM J. Res. Develop.*, vol. 44, no. 3, pp. 323–340, 2000.

[9] ——, "The 'Millipede'—Nanotechnology entering data storage," *IEEE Trans. Nanotechnol.*, vol. 1, pp. 39–55, Jan. 2002.

[10] E. Eleftheriou *et al.*, "'Millipede': A MEMS-based scanning-probe data-storage system," in *Dig. Asia-Pacific Magnetic Recording Conf. 2002, APMRC'02*, vol. CE2, 2002, pp. 01–02.

[11] G. Cherubini *et al.*, "The millipede, a very dense, highly parallel scanning-probe data-storage system," in *Proc. 28th Eur. Solid-State Circuits Conf., ESSCIRC 2002*, 2002, pp. 121–125.

[12] A. Davidson, "MEMS-actuated magnetic probe-based storage," in *Dig. Asia-Pacific Magnetic Recording Conf. 2002, APMRC'02*, vol. CE3, 2002, pp. 01–02.

[13] G. Gibson *et al.*, "U.S. Patent," 5 557 596, 1996.

[14] M. Lutwyche *et al.*, "5 × 5 2D AFM cantilever arrays: A first step toward a terabit storage device," *Sensors Actuators A*, vol. 73, pp. 89–94, 1999.

[15] B. D. Terris, S. A. Rishton, H. J. Mamin, R. P. Ried, and D. Rugar, "Atomic force microscope-based data storage: Track servo and wear study," *Appl. Phys. A*, vol. 66, pp. S809–S813, 1998.

[16] T. Loeliger *et al.*, "CMOS sensor array with cell-level analog-to-digital conversion for local probe data storage," in *Proc. 28th Eur. Solid-State Circuits Conf., ESSCIRC 2002*, 2002, pp. 623–626.

[17] A. H. Sacks, "Position signal generation in magnetic disk drives," Ph.D. dissertation, Carnegie Mellon Univ., 1995.

[18] K. A. S. Immink, *Coding Techniques for Digital Recorders*. London, U.K.: Prentice Hall, 1991.